

LA-UR-15-27728 (Accepted Manuscript)

Fortnightly modulation of San Andreas tremor and low-frequency earthquakes

van der Elst, Nicholas Delorey, Andrew A. Johnson, Paul Allan Shelly, David

Provided by the author(s) and the Los Alamos National Laboratory (2017-01-13).

To be published in: Proceedings of the National Academy of Sciences

DOI to publisher's version: 10.1073/pnas.1524316113

Permalink to record: http://permalink.lanl.gov/object/view?what=info:lanl-repo/lareport/LA-UR-15-27728

Disclaimer:

Approved for public release. Los Alamos National Laboratory, an affirmative action/equal opportunity employer, is operated by the Los Alamos National Security, LLC for the National Nuclear Security Administration of the U.S. Department of Energy under contract DE-AC52-06NA25396. Los Alamos National Laboratory strongly supports academic freedom and a researcher's right to publish; as an institution, however, the Laboratory does not endorse the viewpoint of a publication or guarantee its technical correctness.





Fortnightly modulation of San Andreas tremor and low-frequency earthquakes

Nicholas J. van der Elst^{a,1}, Andrew A. Delorey^b, David R. Shelly^c, and Paul A. Johnson^b

^aEarthquake Science Center, US Geological Survey, Pasadena, CA 91106; ^bGeophysics Group, Los Alamos National Laboratory, Los Alamos, NM 87545; and ^cVolcano Science Center, US Geological Survey, Menlo Park, CA 94025

Edited by Thorne Lay, University of California, Santa Cruz, CA, and approved June 10, 2016 (received for review December 9, 2015)

Earth tides modulate tremor and low-frequency earthquakes (LFEs) on faults in the vicinity of the brittle-ductile (seismic-aseismic) transition. The response to the tidal stress carries otherwise inaccessible information about fault strength and rheology. Here, we analyze the LFE response to the fortnightly tide, which modulates the amplitude of the daily tidal stress over a 14-d cycle. LFE rate is highest during the waxing fortnightly tide, with LFEs most strongly promoted when the daily stress exceeds the previous peak stress by the widest margin. This pattern implies a threshold failure process, with slip initiated when stress exceeds the local fault strength. Variations in sensitivity to the fortnightly modulation may reflect the degree of stress concentration on LFE-producing brittle asperities embedded within an otherwise aseismic fault.

faults | low-frequency earthquakes | tidal triggering | fortnightly tides

S olid Earth tides trigger both earthquakes and tectonic tremor. Tidal triggering of earthquakes is found only for select environments, including shallow thrust faults (1, 2) and midoceanic ridges and transforms (3-5). Tidal triggering of tremor, on the other hand, has been found almost everywhere that tectonic tremor is observed (6–10). Tidal triggering acts as a probe of the properties of faults at depth, generating insights into the mechanics of the brittle-ductile transition (11-16).

Tectonic tremor is believed to result from the superposition of many low-frequency earthquakes (LFEs) occurring on seismic asperities imbedded in an aseismic or creeping medium (17–19). Individual LFE families (spatially localized patches of repeating LFEs) show varying sensitivity to tidal stresses, reflecting heterogeneities in the local stress state, pore pressure, frictional rheology, or other properties (12, 13).

Previous studies have analyzed the amplitude and phase of the semidiurnal tidal modulation of tremor on the San Andreas fault near Parkfield, CA (12, 13) (Fig. 1). Peak LFE rate coincides with the peak semidiurnal shear stress (12). The semidiurnal shear stress is only a few hundred Pascals-six orders of magnitude smaller than the lithostatic stress at the tremor depth of 16–30 km. These observations suggest a very weak fault with high pore pressure and poorly drained hydrologic conditions (12, 13).

The short-period nature of the semidiurnal tides complicates the physical interpretation of triggered LFEs, because the shortterm response may be influenced by the time-dependent process of LFE nucleation (13, 20, 21) or by fault weakening as the tremor episode accelerates (16). To shed additional light on the mechanics of triggering for LFEs and creep episodes, we here analyze the effect of the fortnightly tides, which modulate the semidiurnal tidal amplitude on a 14-d cycle and are relatively far removed from the timescale of LFE nucleation.

Fortnightly modulation has been anticipated, but only recently found, for tectonic earthquakes (22, 23), and it has not yet been investigated for LFEs. The fortnightly tidal cycle can be thought of as the beat frequency arising from the interference between solar and lunar tides. The strongest (spring) tides occur when the moon and sun are aligned, and the weakest (neap) tides occur when the sun and moon are separated by 90°. This pattern results in a ~14-d modulation of the semidiurnal tidal amplitude (Fig. 24).

There are two fundamental ways by which the fortnightly cycle may affect LFE rate, both of which we document in the LFE catalog. The first effect is through the modulation of the amplitude of the peaks and troughs of the semidiurnal tides. Because LFEs correlate more strongly with larger-amplitude shear stress, both the minimum and maximum LFE rates should coincide with the fortnightly peak amplitudes (with $\sim 0^{\circ}$ phase lag). We refer to this as the amplitude effect. Unless the LFE response to positive and negative tides is asymmetrical [which it may be (13, 16)], the 0° fortnightly amplitude effect should average out to be essentially nil on timescales longer than a day.

The second way the fortnightly cycle may modulate LFE occurrence is by modulating the envelope of peak stress (Fig. 24). When combined with the secular tectonic loading rate, the fortnightly tide controls the amount by which the peak stress in each semidiurnal cycle exceeds the peak stress in all previous cycles. This "threshold" effect will show up as enhanced LFE activity during the waxing phase of the fortnightly tide (-90° phase), when the peak stress is most substantially exceeded in each cycle, followed by diminished activity during the waning phase.

Results and Discussion

Amplitude and Phase of the Tidal Modulation. We compute the tidal phase ϕ at the time of occurrence of each LFE. The phase is defined to be 0° at the peak tidal amplitude for both semidiurnal and fortnightly tides, ranging from -180° at the preceding minimum to 180° at the next (1) (Fig. 2A).

Examining all LFE families together, we confirm a 23% semidiurnal modulation of LFE rate (12) with P value << 0.01 by Schuster's test (24). The peak LFE rate has a phase lag of $19^{\circ} \pm 5^{\circ}$

Significance

The sun and moon exert a gravitational tug on Earth that stretches and compresses crustal rocks. This cyclic stressing can promote or inhibit fault slip, particularly at the deep roots of faults. The amplitude of the solid Earth tide varies over a fortnightly (2-wk) cycle, as the sun and moon change their relative positions in the sky. In this study, we show that deep, small earthquakes on the San Andreas Fault are most likely to occur during the waxing fortnightly tide—not when the tidal amplitude is highest, as might be expected, but when the tidal amplitude most exceeds its previous value. The response of faults to the tidal cycle opens a window into the workings of plate tectonics.

Author contributions: N.J.v.d.E., A.A.D., D.R.S., and P.A.J. designed research; N.J.v.d.E. performed research; D.R.S. collected and reduced the seismological data; N.J.v.d.E. performed the tidal analysis; N.J.v.d.E., A.A.D., D.R.S., and P.A.J. analyzed data; and N.J.v.d.E., A.A.D., D.R.S., and P.A.J. wrote the paper.

The authors declare no conflict of interest.

This article is a PNAS Direct Submission.

¹To whom correspondence should be addressed. Email: nvanderelst@usgs.gov.

This article contains supporting information online at www.pnas.org/lookup/suppl/doi:10. 1073/pnas.1524316113/-/DCSupplemental

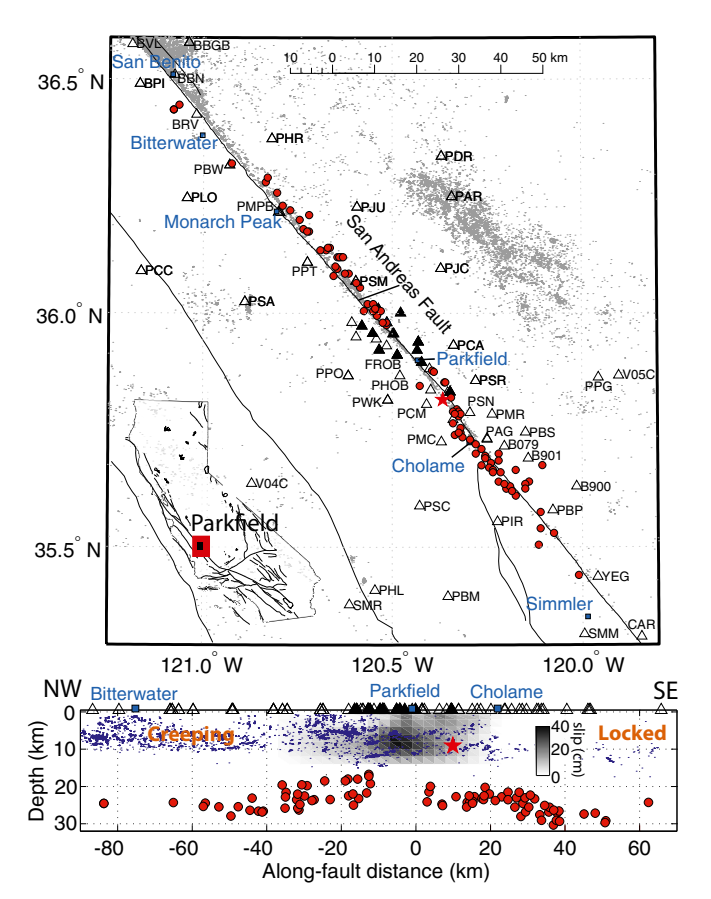


Fig. 1. Location map. Small gray dots are earthquakes; red circles are LFE families. Red star marks the hypocenter of the 2004 Parkfield earthquake. Triangles are seismic stations.

with respect to the semidiurnal tide (Fig. 2B), nearly coincident with the peak tidal stress.

More importantly for this study, we also identify a 6.5% fortnightly modulation, with P value << 0.01 (Fig. 2C). The peak LFE rate has a phase lag of $-90^{\circ} \pm 5^{\circ}$ with respect to the peak fortnightly tide, i.e., coincident with peak fortnightly stressing rate. Enhanced LFE activity is therefore associated with the waxing fortnightly tide, centered on the peak rate of change of the peak stress envelope, and is consistent with the fortnightly threshold effect at -90° .

The fortnightly amplitude effect (expected to peak at 0°) becomes evident when we analyze the positive and negative semidiurnal tides separately. For the negative-only tides, the LFE rate is most suppressed at a fortnightly phase of 0° , as expected (Fig. 2D). For the positive-only semidiurnal tides, LFEs are most strongly encouraged during the late rising phase of the fortnightly tide (-60°). This phase lag falls somewhere between the fortnightly threshold effect (with phase lag -90°), and the fortnightly amplitude effect (with lag near 0°), reflecting the contribution of both.

Variations in Tidal Sensitivity Between LFE Families. Previous studies have found stronger semidiurnal modulation for deeper, more continuously active LFE families than for shallower, more episodic families (12). (We define episodicity as the fraction of the total catalog duration taken up by the largest 2% of the inter-LFE times in each family.) This pattern has been taken as evidence that the fault is weakest near the deep transition between brittle and ductile deformation. We confirm that low-episodicity, more continuous families have a stronger semidiurnal response (Fig. 3A), with modulation amplitude reaching up to 50%. Peak LFE rate roughly

coincides with peak semidiurnal shear stress ($\sim 20^{\circ}$) for nearly all families.

Surprisingly, the amplitude of the fortnightly modulation varies in the opposite direction from the semidiurnal modulation. Lowepisodicity families have weak or insignificant fortnightly modulation, whereas high-episodicity families have a strong modulation—up to 32% (Fig. 3B). All but a few of these families correlate preferentially with the waxing phase of the fortnightly tide, centered on the -90° phase (Fig. 3B). This pattern complicates the interpretation of variations in semidiurnal sensitivity in terms of fault strength alone, but brings an additional observational constraint to bear on the problem.

The observed inverse relationship between semidiurnal and fortnightly sensitivity poses a fundamental mystery: If triggering sensitivity were simply determined by the strength of the fault, we might expect the components of the tidal modulation to scale in the same direction, regardless of their timescale. To understand the differences in fortnightly modulation, we here consider an additional factor, namely the relation between fortnightly stressing and background stressing rate.

Constraints on Stressing Rate from the Fortnightly Modulation. The phase of the correlation between LFE rate and the waxing fortnightly tide (-90°) implies a relatively simple threshold failure process, with LFE episodes most likely to be initiated when the superposition of tectonic and tidal stress exceeds the peak stress in all previous cycles. Another way of saying this is that LFE rate is proportional to stressing rate; $r \propto \dot{r}$. The fact that the phase lag is not shifted substantially from -90° implies that the triggering process is relatively instantaneous compared with the duration of the fortnightly cycle, i.e., there is little delay between the time at which the strength of the fault is first exceeded (slip is initiated) and the time at which slip accelerates to radiate seismic energy as an LFE (slip nucleates).

If threshold failure is indeed instantaneous on the timescale of the fortnight, then changes in the LFE rate will—to the first order—track changes in the stressing rate; $\Delta r \propto \Delta \dot{\tau}$. Because the fortnightly change in shear stressing rate is known, and the percent change in LFE rate can be observed, this scaling relationship can

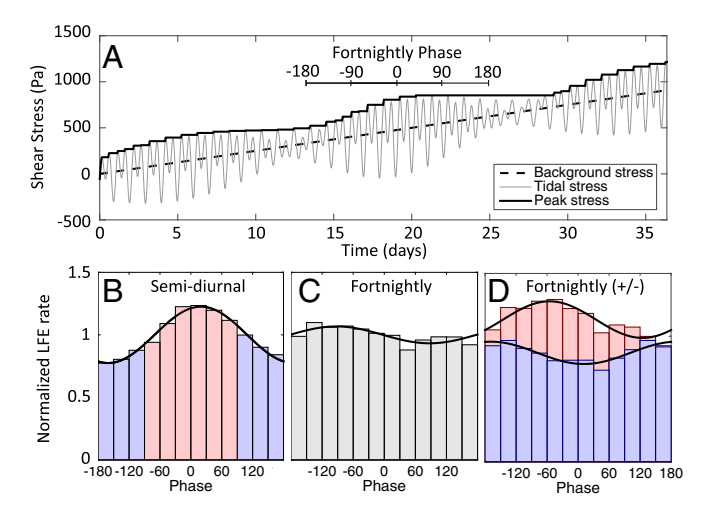


Fig. 2. Fortnightly and semidiurnal tidal modulation of LFEs. (A) Calculated cumulative shear stress on the SAF fault, assuming a background loading rate of 25 Pa/d for purposes of illustration. (B) LFE rate as a function of semidiurnal phase. Colors are for reference in D. (C) LFE rate as a function of fortnightly phase. (D) Fortnightly modulation of LFE rate during positive (red) and negative (blue) semidiurnal tides, respectively. The two histograms sum to give the result in C.

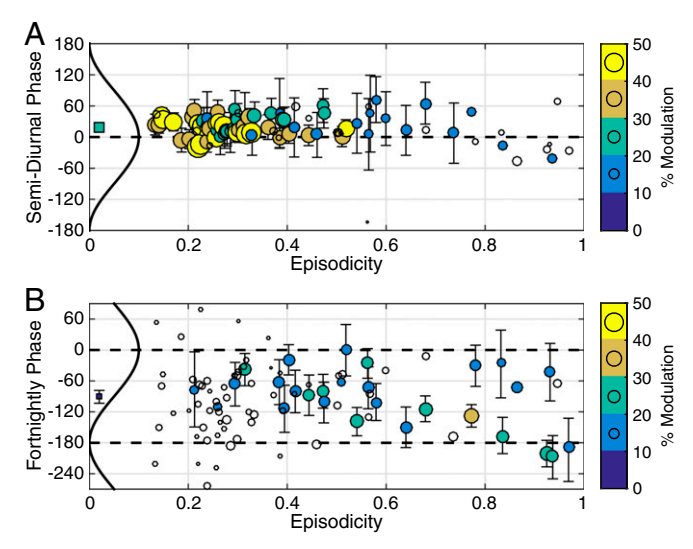


Fig. 3. Phase lag between peak tidal stress and peak LFE rate. Color and symbol size show the amplitude of the modulation. (A) Peak semidiurnal and (B) fortnightly phase of each LFE family as a function of family episodicity. Squares near the left-hand axis give the average over all families. Tidal stress function is shown schematically on the left of each plot; dashed lines are to guide the eye. Error bars give 95% confidence ranges on the phase from the Akaike Information Criterion. Open circles are not significantly different from a uniform distribution according to Schuster's test.

be used to get a rough estimate of the background stressing rate $\dot{\tau}_0$, through the equation

$$\frac{\Delta r}{r_0} = \frac{\Delta \dot{\tau}}{\dot{\tau}_0}.$$
 [1]

The average fortnightly LFE rate modulation $\Delta r/r_0$ is 6.5% (Fig. 2). The fortnightly variation in the stressing rate $\Delta \dot{\tau}$ is calculated to be about 35 Pa/d (*Materials and Methods*). Plugging these values into Eq. 1 gives an average background stressing rate $\dot{\tau}_0$ of about 535 Pa/d.

The simplest interpretation of $\dot{\tau}_0$ is in terms of shear stressing rate, given the dominant role of shear stresses found in prior studies of tidal triggering on the San Andreas (10, 12, 16). Alternatively, $\dot{\tau}_0$ can be thought of more generally as the background rate of approach to failure, including the effect of shear stress, normal stress, pore pressure, and fault healing and weakening. The fortnightly modulation should then be taken to reflect the relative contribution of tidal shear stress compared with background loading processes in driving asperities to failure. With this in mind, the simplified stressing rate estimates of Eq. 1 should be considered a first-order approximation or an upper bound on the rate of actual shear stress accumulation on the LFE asperities.

The amplitude of the fortnightly modulation across LFE families varies from 1% to 32% between families, with the larger values for the more episodic families (Fig. 3). Through the logic of Eq. 1, this variability implies average background stressing rates (or rates of approach to failure) between 110 Pa/d and about 3,500 Pa/d, with the smaller value for the more episodic families. Plotting the apparent loading rate in cross-section suggests a pattern (Fig. 4); background stressing rate is highest for families at the margins of the LFE-producing regions, and smallest for families in the interior of these regions.

A long-term secular stressing rate in the range of 3,500 Pa/d is hard to justify over large regions, as it should lead to a 1-MPa stress drop event every year. This value is considerably larger than the stressing rate implied by the Parkfield earthquakes (and afterslip), which relieve only about 1 MPa per 30 y (25),

consistent with the much smaller 110 Pa/d range measured for the most episodic families. Because we only measure apparent background stressing rate for active LFE-producing regions, the higher than expected stressing rate could be explained by temporal variations in the transient slow-slip rate itself. However, the highest apparent stressing rates are observed for the most regular and continuous LFE families. If fluctuating transient slip rate explained all of the variation in apparent stressing rate, it would require the background slip rate to be most irregular for the most regular LFE families—a less than satisfying conclusion.

A better explanation may be that the apparently elevated stressing rate reflects the concentration of the load onto isolated LFE patches embedded within a weak aseismic medium (26). Because previous researchers found the semidiurnal response to be dominated by fault-parallel shear stress (10, 12, 16), we here interpret the background stressing rate in terms of shear stressing rate. For isolated LFE patches under ideal conditions, the amount of shear stress concentration should be inversely proportional to the size of the LFE patch (26). For more complicated distributions of weakly interacting asperities, the picture may be more complex, but the direction of the scaling persists—smaller and more isolated patches will experience greater stress concentration. In this interpretation, variations in tidal sensitivity reflect the heterogeneous and patchy approach to the brittle—ductile transition.

The ~110 Pa/d stressing rate estimated for the most episodic LFE families is a plausible upper bound on the long-term tectonic shear stressing rate. According to the stress concentration interpretation, the episodic LFE families would then reflect regions made up primarily of brittle LFE-generating fault, with little stress concentration. Conversely, the much higher apparent stressing rates inferred for the least episodic LFE patches would indicate a lower proportion of brittle to assismic fault patches, with proportionally higher stress concentration. If this explanation is correct, then the most continuous LFE families have a concentration factor up to ~30 compared with the most episodic families, implying that the average scale length of the brittle asperities is something on the order of 30 times smaller.

As a final comment, if the background stressing rate is approximately constant between successive LFE episodes, then multiplying the background stressing rate by the typical recurrence times for an LFE family gives an estimate of the stress accumulated on the LFE asperity between slip episodes. Taking the mean of the largest 0.1% of interevent times as an upper bound on the recurrence time for each family, we estimate stress accumulations of 3–30 kPa per episode (Fig. 5). The stress accumulation (and hence stress drop) for each family appears to be relatively independent of stressing rate or recurrence time The stress drop estimate of 3–30 kPa compares favorably with the 10–100 kPa per episode estimated for tremor and slow-slip episodes in Cascadia, where the recurrence time is 12–14 mo (27).

Relationship Between the Semidiurnal and Fortnightly Modulations.

Although the -90° phase shift for the fortnightly modulation suggests a relatively simple threshold failure model on the timescale of the fortnight, this simple threshold model cannot simultaneously explain the semidiurnal modulation, which is peaked near 0° with respect to the peak stress (Fig. 2B).

Two basic models have been put forward to explain the phase of the semidiurnal modulation. The first model comes from laboratory studies of friction, and posits that LFEs have a nucleation phase, in that the transition from locked to sliding occurs via a stress-driven acceleration of slip with some nonzero duration in time (12, 13, 20, 21). If the duration of the accelerating slip phase is longer than the period of the semidiurnal tides, LFE patches will survive multiple stress cycles before ultimately failing, and the peak LFE rate will coincide with the peak tidal stress. This model has had great success in describing the behavior of laboratory earthquakes (20, 21). In the second model, LFEs occur by simple

van der Elst et al. PNAS Early Edition | 3 of 5

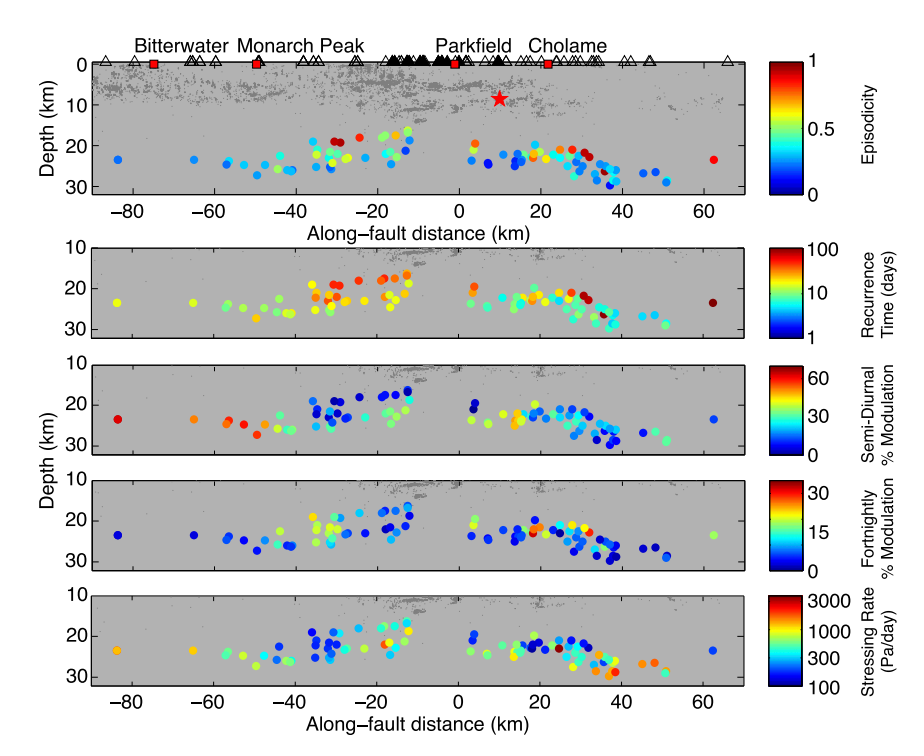


Fig. 4. Cross-sections of measured and estimated parameters for LFE families on the San Andreas Fault. Northwest is to the left. Colored dots are LFE families; small gray dots are upper crustal earthquakes. The red star is the 2004 Parkfield earthquake hypocenter. Seismic stations are marked by triangles.

threshold failure, but are driven indirectly by tidally modulated creep in the encompassing fault zone, which results in the overall rate being again in phase with the tidal stress (12, 13, 16). The latter model is consistent with the pulse-like quality of the LFE episodes, and with observations in other regions (e.g., Cascadia) that find a correspondence between tremor and geodetically observed slow slip (12, 13, 16).

Regardless of which semidiurnal triggering model is correct, the inverse relationship between the strength of the semidiurnal and fortnightly modulations provides a key insight into the mechanics of LFEs and the structure of the deep fault. Based on the phase of the two tidal correlations, we infer that the amplitude of the fortnightly modulation reflects variations in stress concentration on LFE asperities, and the amplitude of the semidiurnal modulation reflects variations in overall fault strength. The more continuous LFE families have high semidiurnal sensitivity and low fortnightly sensitivity, suggesting low overall fault strength and high apparent stressing rate (high stress concentration). These two observations are consistent with the more continuous LFEs being generated on isolated asperities within an otherwise aseismic, weak creeping fault zone. The more episodic families, on the other hand, have low semidiurnal sensitivity and high fortnightly sensitivity, suggesting higher overall fault strength and lower stress concentration. This pattern is consistent with larger, more contiguous LFE asperities.

Overall, the observations paint a picture consistent with the idea that the brittle-ductile transition is gradational and heterogeneous, with LFE-producing asperities becoming smaller and more isolated as the transition to aseismic deformation becomes more complete. The inverse relationship between the LFE responses observed at two different tidal timescales should serve as a powerful constraint on future models of the rheology and mechanics of the deep San Andreas.

Materials and Methods

Calculation of the Tidal Shear Stress. We use Duncan Agnew's tidal code package SPOTL (subroutine *ertid*) to calculate the solid Earth tides (28). This

subroutine computes tides for the second and third lunar harmonics and the second solar harmonic, which is adequate, given our focus on the average response at semidiurnal and fortnightly periods. The ocean loading component can be neglected for this section of the San Andreas (10). We assume that the coefficient of friction is near zero, based on previous estimates (10) of $\mu=0.02$, and look only at the fault-parallel shear stress in the semidiurnal tidal analysis. The fortnightly tide modulates all components of the tidal stress, and is therefore not specific to any particular component.

In computing fault shear stress, we assume linear elasticity, plane strain, a Poisson's ratio of 0.25, and a shear modulus of 30 GPa. We resolve the tidal shear stress on a vertically dipping, right-lateral fault with azimuth 315°. Because the fortnightly cycle modulates all components of the tidal strain

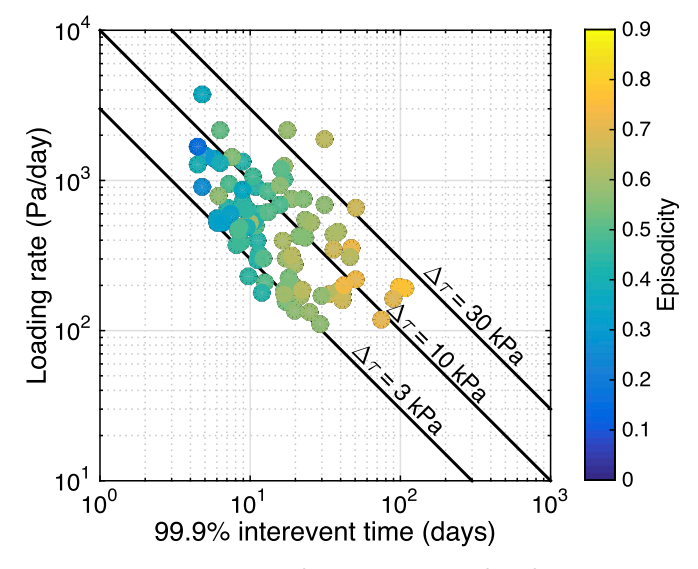


Fig. 5. Loading rate estimated from the amplitude of the fortnightly modulation, against maximum recurrence time for each LFE family. Black lines are contours of constant stress accumulation (stress drop) per episode.

tensor in the same way, there should be minimal sensitivity to small inaccuracies in the stress tensor (22). Unfortunately, this insensitivity also limits our ability to measure the relative contributions of the normal and shear stress components of the tidal stress tensor. For a more careful analysis of the relationship between the tidal stress tensor and the semidiurnal LFE rate modulation, we direct the interested reader to previous studies (10, 12).

The semidiurnal phase is calculated following ref. 1. We high-pass filter the calculated tidal shear stress (two-pole Butterworth, 12-h corner). This filtering damps out the fortnightly signal, and ensures that there is a well-defined minimum and maximum for each semidiurnal cycle. The distribution of the semidiurnal phase, so defined, is not entirely uniform for random times (Fig. S1). We therefore normalize the semidiurnal LFE rate histogram (Fig. 2) by the baseline distribution in Fig. S1; this is for plotting purposes only. The fluctuations in the baseline phase distribution have period equal to exactly one-half the semidiurnal period (Fig. S1), meaning there is no net contribution of this baseline nonuniformity to the cosine fit at the full semidiurnal period.

The fortnightly phase is calculated for the times of the LFEs, assuming the fortnightly amplitude is described by a cosine function with period equal to half the lunar synodic period, i.e., $2T_{fn}=29.530589$ d. The fortnightly phase is a linear function of time $\phi_{fn}\equiv \text{mod}(\phi_0+360\cdot t/T_{fn},360)-180$. The amplitude $\Delta\dot{\tau}=35$ Pa/d and initial phase ϕ_0 of the fortnightly oscillation are found by stacking all of the fortnightly cycles and fitting a cosine to the 90% quantile of the shear stress. The 90% quantile is very well modeled by a cosine function, with absolute residual ≤ 2.7 Pa.

Fitting Amplitude and Phase of the Tidal Modulation. We fit the distribution of LFE phases to a cosine function by maximum likelihood. The 95% confidence range on the phase lag between tidal stress and LFE rate is defined as the range of phases for which the sample likelihood is greater than 95% of the maximum. Populations of LFEs for which 95% confidence bounds on the cosine phase do not exist are considered insignificantly different from a uniform distribution. The number of events in each LFE family is variable; this can affect the ability to resolve a significant signal, but it does not introduce systematic bias into the estimate of amplitude and phase of the modulation (Fig. S2).

We also apply Schuster's test (24) to establish significance of the tidal modulation. This test treats the occurrence of each LFE as a unit step on a

polar diagram in the direction of the instantaneous tidal phase (LFE phase). The norm of the vector sum D of these steps is a random walk in the absence of a tidal modulation. The total deviation away from the origin is a measure of the strength of the modulation, with probability $P = \exp(-D^2/N)$ of exceeding distance D by chance in N steps. Schuster's test gives no information about the phase or amplitude of the modulation but is somewhat more stringent than the 95% likelihood test. The tidal correlation for an LFE family must pass both Schuster's test (P < 0.05) and the 95% maximum likelihood test to be included.

LFE Catalog. We use the LFE catalog spanning the years 2008–2015, which includes ~4 million discrete LFEs belonging to 88 different families (19). This time period is chosen to be well outside the time affected by the 2004 Parkfield earthquake. We characterize the LFE families based on episodicity, using a metric similar to Shelly and Johnson (29), which allows us to rank LFE families according to how burst-like the activity tends be. We define episodicity as the fraction of the total catalog duration taken up by the largest 2% of the inter-LFE times.

Statistical tests for tidal correlations assume that the LFEs are independent and identically distributed in the absence of any modulation (i.e., would be uniformly distributed). In actuality, LFEs are clustered, especially for the more episodic families. We therefore apply a simple declustering algorithm in which we count only the first LFE per family per 1-h period. The declustering limits the degree to which a single large burst can dominate the tests for significance, and allows for more precise measurements of the amplitude and phase of the tidal modulation. The declustering leaves 81,000 of the LFEs (21% of the original catalog). The major conclusions of this study do not depend on the declustering (Figs. S3 and S4).

ACKNOWLEDGMENTS. This paper benefitted from discussions with Robert Guyer, Tom Heaton, Victor Tsai, Nicholas Beeler, and Elizabeth Cochran; the latter two also provided early reviews of the manuscript. We also thank Heidi Houston, an anonymous reviewer, and editor Thorne Lay for helpful reviews and comments. This work was supported by a grant from Los Alamos National Laboratory and the US Geological Survey Mendenhall program. Any use of trade, firm, or product names is for descriptive purposes only and does not imply endorsement by the US Government.

- Tanaka S, Ohtake M, Sato H (2002) Evidence for tidal triggering of earthquakes as revealed from statistical analysis of global data. J Geophys Res Solid Earth 107 (B10):2211.
- Cochran ES, Vidale JE, Tanaka S (2004) Earth tides can trigger shallow thrust fault earthquakes. Science 306(5699):1164–1166.
- Wilcock WS (2001) Tidal triggering of microearthquakes on the Juan de Fuca Ridge. Geophys Res Lett 28(20):3999–4002.
- Stroup D, Bohnenstiehl D, Tolstoy M, Waldhauser F, Weekly R (2007) Pulse of the seafloor: Tidal triggering of microearthquakes at 9° 50'N East Pacific Rise. Geophys Res Lett 34(15):L15301.
- Métivier L, et al. (2009) Evidence of earthquake triggering by the solid Earth tides. Earth Planet Sci Lett 278(3):370–375.
- Gomberg J, et al. (2008) Widespread triggering of nonvolcanic tremor in California. Science 319(5860):173.
- Lambert A, Kao H, Rogers G, Courtier N (2009) Correlation of tremor activity with tidal stress in the northern Cascadia subduction zone. J Geophys Res Solid Earth 114(B8):B00A08.
- Nakata R, Suda N, Tsuruoka H (2008) Non-volcanic tremor resulting from the combined effect of Earth tides and slow slip events. Nat Geosci 1(10):676–678.
- Rubinstein JL, La Rocca M, Vidale JE, Creager KC, Wech AG (2008) Tidal modulation of nonvolcanic tremor. Science 319(5860):186–189.
- Thomas AM, Nadeau RM, Bürgmann R (2009) Tremor-tide correlations and nearlithostatic pore pressure on the deep San Andreas fault. Nature 462(7276):1048–1051.
- Rubinstein JL, Shelly DR, Ellsworth WL (2010) Non-volcanic tremor: A window into the roots of fault zones. New Frontiers in Integrated Solid Earth Sciences, eds Cloetingh SAPL, Negendank J (Springer, New York), pp 287–314.
- Thomas AM, Bürgmann R, Shelly DR, Beeler NM, Rudolph ML (2012) Tidal triggering of low frequency earthquakes near Parkfield, California: Implications for fault mechanics within the brittle-ductile transition. J Geophys Res Solid Earth 117(B5): R05301
- Beeler NM, Thomas AM, Bürgmann R, Shelly DR (2013) Inferring fault rheology from low-frequency earthquakes on the San Andreas. J Geophys Res Solid Earth 118(11): 5976–5990.
- Ide S (2010) Striations, duration, migration and tidal response in deep tremor. Nature 466(7304):356–359.
- Ide S (2012) Variety and spatial heterogeneity of tectonic tremor worldwide. J Geophys Res Solid Earth 117(B3):B03302.

- Houston H (2015) Low friction and fault weakening revealed by rising sensitivity of tremor to tidal stress. Nat Geosci 8(5):409–415.
- Obara K (2002) Nonvolcanic deep tremor associated with subduction in southwest Japan. Science 296(5573):1679–1681.
- Shelly DR, Beroza GC, Ide S, Nakamula S (2006) Low-frequency earthquakes in Shikoku, Japan, and their relationship to episodic tremor and slip. Nature 442(7099): 188–191
- Shelly DR, Hardebeck JL (2010) Precise tremor source locations and amplitude variations along the lower-crustal central San Andreas Fault. Geophys Res Lett 37(L14): L14301.
- Beeler NM, Lockner DA (2003) Why earthquakes correlate weakly with the solid Earth tides: Effects of periodic stress on the rate and probability of earthquake occurrence. J Geophys Res Solid Earth 108(B8):2391.
- Savage HM, Marone C (2007) Effects of shear velocity oscillations on stick-slip behavior in laboratory experiments. J Geophys Res 112(B2):B02301.
- 22. Hartzell S, Heaton T (1989) The fortnightly tide and the tidal triggering of earth-quakes. *Bull Seismol Soc Am* 79(4):1282–1286.
- Bhatnagar T, Tolstoy M, Waldhauser F (2016) Influence of fortnightly tides on earthquake triggering at the East Pacific Rise at 9°50'N. J Geophys Res Solid Earth 121(3):1262–1279.
- Schuster A (1897) On lunar and solar periodicities of earthquakes. Proc R Soc London 61(369-377):455–465.
- Murray J, Langbein J (2006) Slip on the San Andreas Fault at Parkfield, California, over two earthquake cycles, and the implications for seismic hazard. Bull Seismol Soc Am 96(4B):S283–S303.
- Johnson LR, Nadeau RM (2002) Asperity model of an earthquake: Static problem. Bull Seismol Soc Am 92(2):672–686.
- Schmidt DA, Gao H (2010) Source parameters and time-dependent slip distributions
 of slow slip events on the Cascadia subduction zone from 1998 to 2008. J Geophys Res
 Solid Earth 115(B4):B00A18.
- Agnew DC (2012) SPOTL: Some Programs for Ocean-Tide Loading (Scripps Inst Oceanogr, San Diego).
- Shelly DR, Johnson KM (2011) Tremor reveals stress shadowing, deep postseismic creep, and depth-dependent slip recurrence on the lower-crustal San Andreas fault near Parkfield. Geophys Res Lett 38(13):L13312.

van der Elst et al. PNAS Early Edition | **5 of 5**

Supporting Information

van der Elst et al. 10.1073/pnas.1524316113

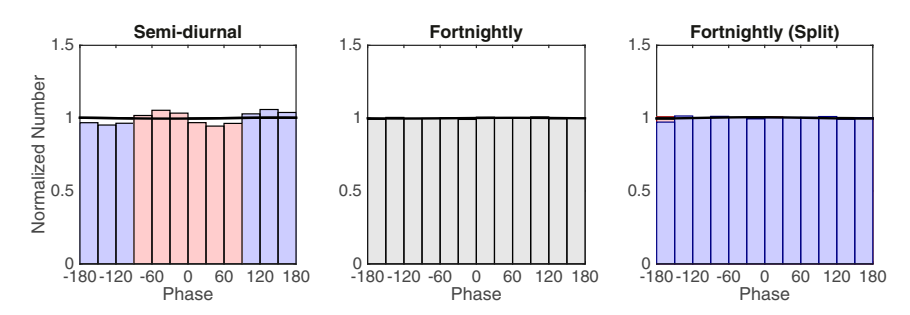


Fig. S1. Tidal correlations for a random time series (compare with Fig. 2). Black line is the cosine fit. The small nonuniformity of the semidiurnal phase distribution does not contribute to the cosine fit at the period of the tides.

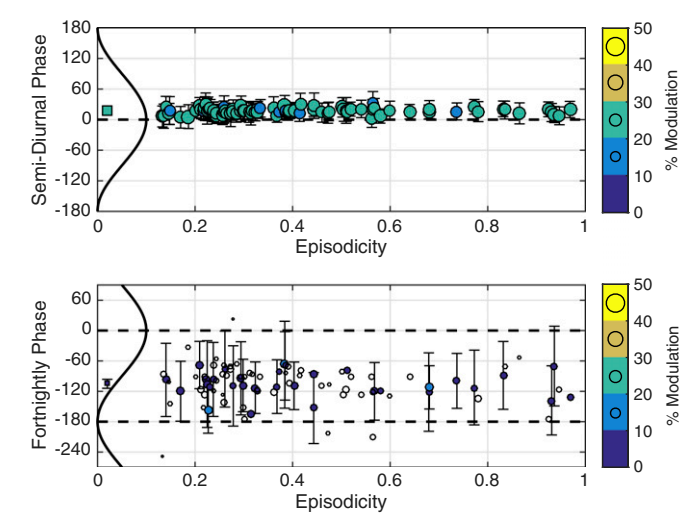


Fig. S2. Tidal phase as a function of LFE family for a catalog of reshuffled LFE times (compare with Fig. 3). No systematic variation is seen between families (although the average signal remains); this shows that the observed trend is not simply a function of sample size.

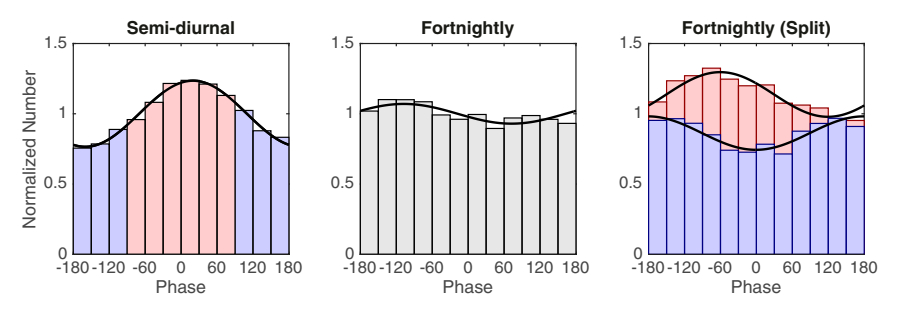


Fig. S3. Tidal correlations for the raw, undeclustered LFE catalog (compare with Fig. 2). Amplitude and phase are negligibly different from the declustered catalog.

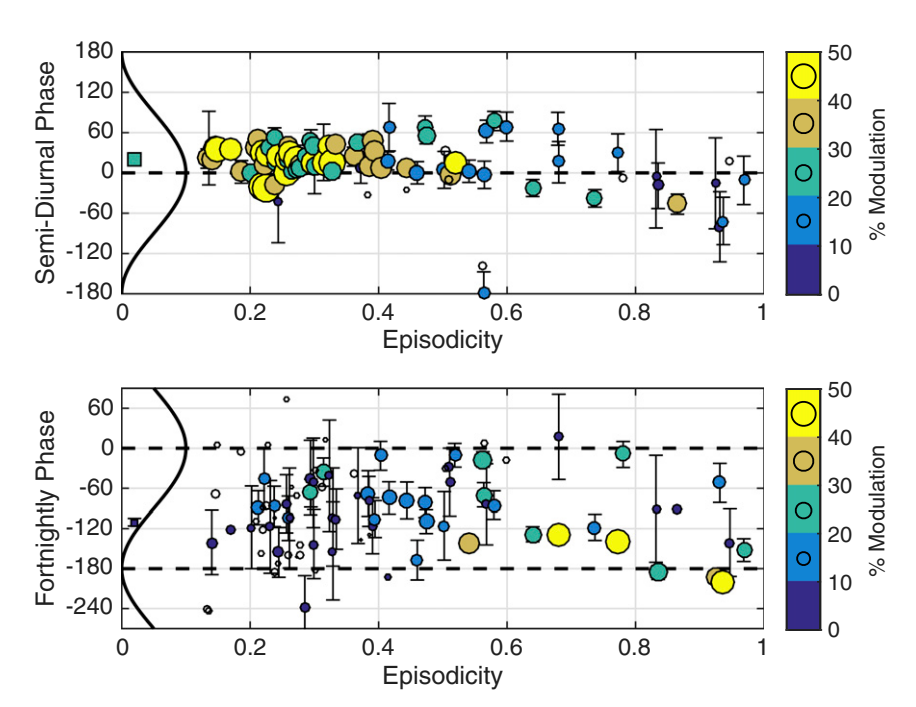


Fig. S4. Tidal phase as a function of LFE family episodicity for the raw (undeclustered) catalog. Compare with Fig. 3.